Int. J. Electrochem. Sci., 10 **(2015)** 8982 - 8992

International Journal of
ELECTROCHEMICAL
SCIENCE
www.electrochemsci.org

Mesoporous Carbon Supported Cobalt and Iron Binary Hydroxide Catalyst for Cathode in Non-aqueous Li-air Batteries

Imgon Hwang[1], *Gibaek Lee*[1,2], *Yongsug Tak*[1,*]

[1]Department of Chemical Engineering, Inha University, 253 Yonghyun-dong, Nam-ku, Incheon 402 751, Republic of Korea
[2]Department of Physics, Martin-Luther University of Halle-Wittenberg, Halle (Saale) 06099, Germany
[*]E-mail: ystak@inha.ac.kr

Received: 12 August 2015 / *Accepted:* 11 September 2015 / *Published:* 30 September 2015

The rechargeable Li-air battery represents an attractive energy storage device for various applications because of its theoretical energy storage capacity (~3000 Wh/kg) compared with that of Li-ion batteries. However, the efficiency of Li-air batteries is limited by the large cathodic overpotential for oxygen reduction reaction (ORR) and oxygen evolution reaction (OER). This article demonstrates that a binary hydroxide catalyst composed of iron (Fe) and cobalt (Co) supported on mesoporous carbon material such as CMK-3 can address this problem with a non-aqueous electrolyte of 1M LiTFSI in TEGDME. The mesoporous $Co(OH)_2$-$Fe(OH)_2$/CMK-3 catalyst showed remarkable overpotential reduction and achieved a fairly stable cyclability for 20 cycles at 0.2 mA/g compared with the carbon black support. Moreover, the physical analysis confirms that the feature of mesoporous structure is beneficial to the diffusion of oxygen during the discharge process and the decomposition of discharge products during the charge process.

Keywords: Li-O_2 battery, mesoporous carbon, CoO/FeO/CMK-3, non-aqueous electrolyte, binary catalyst

1. INTRODUCTION

Using lithium ion batteries in electric portable applications is limited by a number of problems such as insufficient gravimetric energy, specific power density, and poor lithium ion intercalation at cathode [1-5]. Therefore, in order to remedy the shortcomings, Li-O_2 battery was proposed to substitute the intercalation material of cathode, leading to the higher energy storage capacity with the catalytically active oxygen reduction in comparison with the lithium ion batteries [6]. However, Li-O_2 battery has disadvantages including large overpotential, low cycleability and low rate capability during

charge-discharge process in commercial applications. Most of all, it is very important to develop the electrocatalyst which is able to decrease the overpotential of oxygen reduction and the evolution reaction during the cycling since Li anode has very little polarization.

In many studies, they have made efforts to adapt cathode catalysts of Li-air batteries. Novel-metals, Pt-based catalysts, show a high activity during charge process, but have a problem with expensive price [7-10]. Therefore, many researches have tried to develop new catalysts using non-precious metal instead of Pt-based precious metal [11-12]. Especially, catalysts involving Fe, Co, and Mn show a high catalytic activity in oxygen evolution reaction during charge process [13-16]. Furthermore, the structure of mainly carbon as a support material of catalysts plays a critical factor to suppress the overpotential during charging and discharging in electrochemical performance of Li-air batteries [17]. Insoluble product formed during the discharge process is not completely decomposed during charge process.

$2Li^+ + 2e^- + O_2 \rightarrow Li_2O_2$ discharge product

$Li_2O_2 \rightarrow 2Li^+ + 2e^- + O_2$ decomposition process

On the contrary, the product is accumulated on the surface of catalyst, leading to decrease catalytic active site, cycleability and cell potential owing to the hindrance of oxygen diffusion [18].

In this work, we prepared cobalt and iron binary hydroxides as a cathode catalyst and mesoporous carbon material, CMK-3, as a support material using modified polyol method, which is in the interest of reducing the cell overpotential and the discharging product, leading to improvement of cycleability and capacity retention. CMK-3 shows a high electroactive surface area and a good electrochemical performance induced by a very specially ordered and interconnected pore structure [19-20]. The synthesized catalyst was analyzed by the physicochemical characterization, and confirmed by the cell overpotential and the cycleability using a non-aqueous electrolyte of 1M LiTFSI in TEGDME. Also, in order to identify formation and decomposition of discharge products, Li_2O_2 and Li_2CO_3, we conducted X-ray spectroscopy (XRD), fourier-transform infrared spectroscopy (FT-IR), and electrochemical impedance spectroscopy (EIS) before and after charge-discharge process.

2. EXPERIMENTAL

2.1.1. Synthesis of mesoporous SBA-15 and CMK-3

Mesoporous carbon (CMK-3) was prepared by wet impregnation method using mesoporous silica (SBA-15) as a support material [21]. SBA-15 was synthesized by the following procedure [22]. 4.0 g Pluronic P123 (polyethylene oxide-polypropylene oxide-polyethylene oxide, $EO_{20}PO_{70}EO_{20}$) was mixed with 120 mL distilled water and 25 mL hydrochloric acid, followed by stirring vigorously for 1 hr. 9.1 mL TEOS (tetraethyl orthosilicate) as a silica precursor was added in the mixture and placed in an oven for 20 hr at 308 K. The product was washed with distilled water and EtOH. Afterward, it was dried at 323 K and finally calcined for 5 hr at 823 K.

CMK-3 was synthesized according to a literature procedure [21]. 1 g SBA-15 was dispersed with 1.25 g sucrose as a carbon precursor and 0.07 mL H_2SO_4, and the result solution was impregnated for 1 hr at 373 K and for 6 hr at 433 K. After this process again, the mixture was conducted by the carbonization process with heating to 1173 K under Ar environment. Finally, silica template of the product was removed by 5 wt % of HF solution, followed by washing with EtOH several times and drying at 353 K oven completely.

2.1.2. Synthesis of $Co(OH)_2$-$Fe(OH)_2$/CMK-3 catalyst

The binary hydroxides supported on CMK-3, $Co(OH)_2$-$Fe(OH)_2$/CMK-3, catalyst was prepared by using modified polyol method [23]. Cobalt (anhydrous $CoCl_2$) and iron ($FeCl_2 \cdot 4H_2O$) precursors were each dissolved in 50 mL ethylene glycol. The solutions containing cobalt and iron were mixed thoroughly to obtain homogeneous mixture using ultrasonic stirring. 500 mg CMK-3 was dissolved in 250 mL ethylene glycol and dispersed homogeneously with the same method. Two solutions were mixed and added 1 M NaOH to adjust the pH of the solution to 9.5, followed by heating at 160˚C for 3 hours with stirring vigorously. Afterward, the solution was stirred for 24 hr at room temperature. Finally, the result product was centrifugally separated and then dried in an oven at 110˚C for overnight.

2.2 Physical characterization

The structure and crystallinity of prepared catalyst was analyzed by wide angle X-ray spectroscopy (WAXS, Rigaku, D/max-2200), small angle X-ray spectroscopy (SAXS, Rigaku, D/max-2500) analysis. The weight of the metal hydroxides supported on CMK-3 was confirmed by thermogravimetry analysis (TGA, PERKIMELMER, TG/DTA 6300). The element distribution and weight of CMK-3 supported cobalt and iron hydroxides was examined by transmission electron microscopy (TEM, JEOL, JEOL-2100F) and EDX (energy dispersive X-ray spectroscopy) mapping.

2.3 Electrochemical cell and characterization

The electrochemical cell performance was conducted on a Swagelok-type cell. It was assembled in argon-filled glove box where the moisture and oxygen concentration were less than 1 ppm. Swagelok-type Li-air cell was composed of a lithium metal as a anode, impregnated non-aqueous electrolyte, such as 1 M LiTFSI (lithium bis(trifluoromethanesulfonyl)imide) in TEGDME (tetraethylene glycol dimethyl ether), and a catalyzed porous as air-cathode. A glass fiber separator was placed between two electrodes. The $Co(OH)_2$-$Fe(OH)_2$/CMK-3 catalyst was used as the air electrode of Li-air battery. It was completely dispersed with isopropyl alcohol and sprayed onto gas diffusion layer (GDL, 10BC, SIGRACET®) loaded with 1 mg/cm^2. Cut-off capacity of charge-discharge cycles was conducted to investigate cycle stability, reversible capacity, and plateau voltage at 700 mAh/g. The constant current density of discharge and charge cycle test was applied at 0.2 mg/cm^2 (157 mA/g). Discharge product which was formed and discomposed during cycling was

confirmed by using X-ray diffraction (XRD, Rigaku, D/max-2200), fourier transform infrared Spectroscopy (FT-IR, Bruker, VERTEX 80V) and the electrochemical impedance spectroscopy (EIS) (PGSTAT302N, FRA2 module), respectively.

3. RESULTS AND DISCUSSION

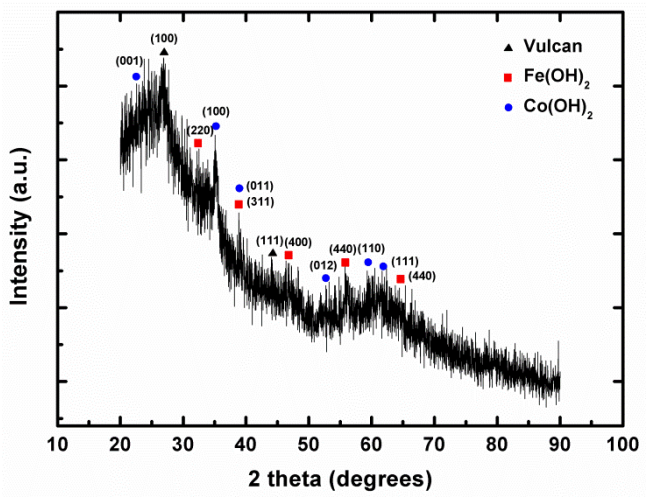

A

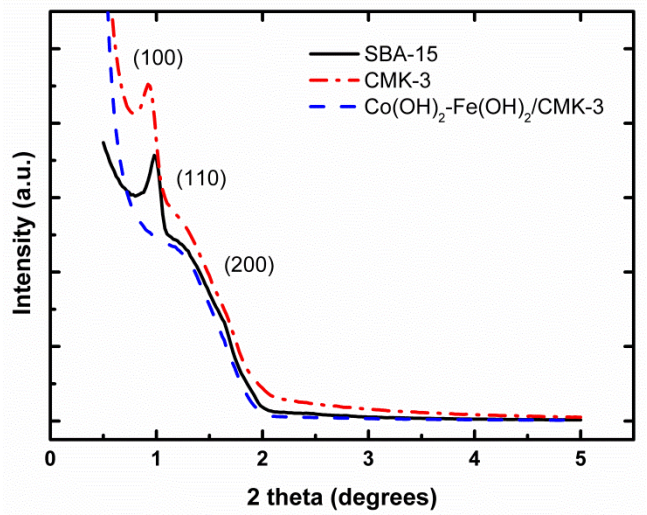

B

Figure 1. (a) Wide angle X-ray diffraction (WAXS) of prepared $Co(OH)_2$-$Fe(OH)_2$/CMK-3 catalyst by modified polyol method. (b) Small angle X-ray diffraction (SAXS) patterns of SBA-15, CMK-3, and $Co(OH)_2$-$Fe(OH)_2$/CMK-3 catalysts.

The crystallinity of mesoporous carbon (CMK-3)-supported $Co(OH)_2$-$Fe(OH)_2$ catalyst was analyzed by XRD measurement as shown in Fig. 1. WAXS (wide angle X-ray spectroscopy) of Fig. 1a confirmed that cobalt and iron metals presented hydroxide structures such as CoO and FeO, and the intensity of low peak may result from small crystal size of particles in hydroxides [24]. SAXS (small

angle X-ray spectroscopy) measurement demonstrated that all synthesized SBA-15, CMK-3, and $Co(OH)_2$-$Fe(OH)_2$/CMK-3 catalyst were formed with high ordered mesoporous structure (p6mm) as shown in Fig. 1b [21]. The (100) peak of $Co(OH)_2$-$Fe(OH)_2$/CMK-3 catalyst was disappeared because cobalt and iron hydroxides nanoparticles which formed after impregnation process were partially filled with channels of CMK-3 [25]. CMK-3 was a very adaptable for air electrode of Li-air batteries as a support material because its mesoporous structure can be maintained without collapsing although the portions of channels were filled by cobalt and iron hydroxides [25].

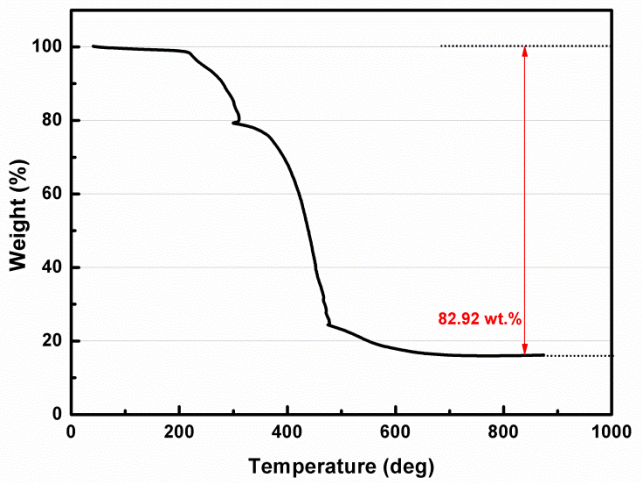

Figure 2. Thermogravimetry analysis (TGA) of $Co(OH)_2$-$Fe(OH)_2$/CMK-3 catalyst.

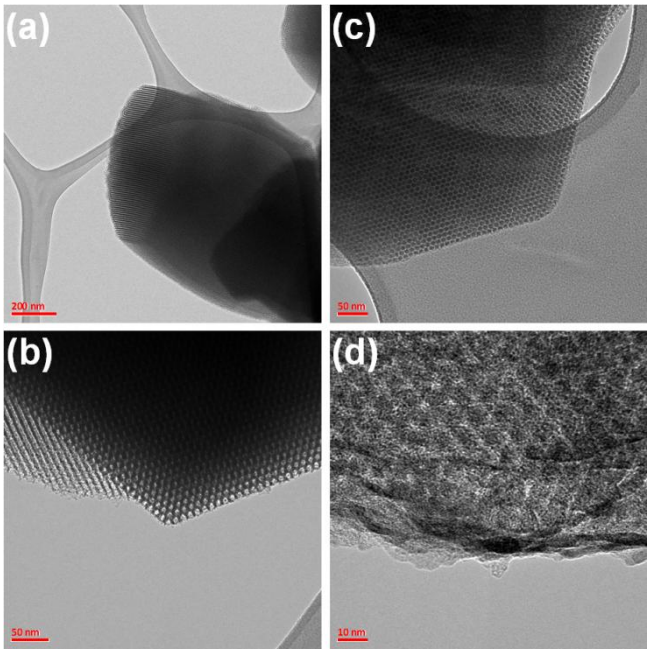

Figure 3. TEM images of (a), (b) SBA-15, (c) and (d) CMK-3 nanoparticles.

The total weight percent of cobalt and iron hydroxides supported CMK-3 was 17.08 wt % analyzed by TGA measurement as shown in Fig. 2. After the water desorption, the dehydration process of $Co(OH)_2$ and $Fe(OH)_2$ into Co_3O_4 and Fe_3O_4 was taken place between 220 and 280˚C, respectively [26,27]. Rapid weight loss until 550˚C can be mainly attributed to the carbon combustion.

In order to find out the size of cobalt and iron hydroxide nanoparticles as based on the WAXS data of Fig. 1a, distributions and atomic weight percent of elements were analyzed by TEM and EDX mapping. Fig. 3 shows TEM images of typical SBA-15 and CMK-3. The structure of SBA-15 consisted of hexagonal arrays, honeycomb-like shape with the cylindrical mesoporous tube (around 9 nm of pore diameter) as shown in Fig 3(a, b). On the other hand, the structure of CMK-3 (around 7 nm of pore diameter) was almost exact replica of SBA-15. The morphologies are quite similar in both CMK-3 carbon and SBA-15 silica particles. The carbon structures, thus, formed uniformly throughout the entire volume of SBA-15 particle and the pore of SBA-15 can be filled up with carbon particles by infiltration. The dispersion element of cobalt and iron hydroxides on CMK-3 support was characterized by EDX mapping as shown in Fig 4.

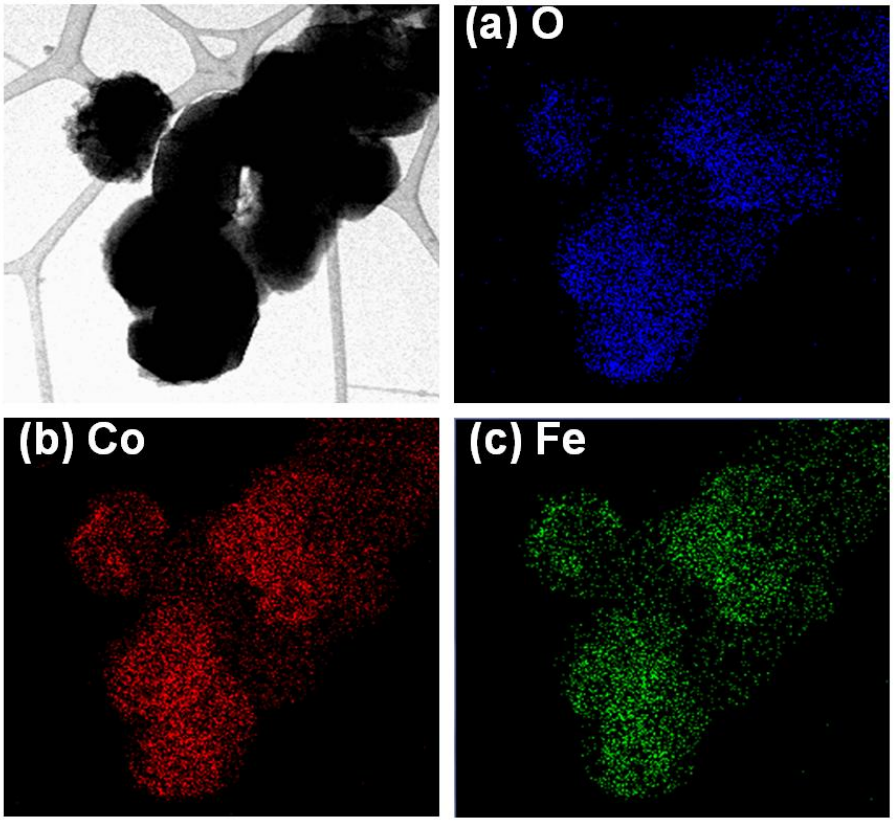

Figure 4. TEM image of $Co(OH)_2$-$Fe(OH)_2$/CMK-3 catalyst showing where the elemental maps were obtained. Mappings of the elements (a) Oxygen, (b) Cobalt, and (c) iron elements.

The blue color indicates the element of oxygen (Fig. 4a), the red color shows the element of cobalt (Fig. 4b), and the green color shows the element of iron (Fig. 4c). It can be confirmed that the particle sizes of individual elements are well distributed without agglomeration and concentration to

one side. In addition, the weight percent of cobalt, iron, and oxygen elements of total catalyst confirmed 6.49, 3.18, and 9.54 wt %, respectively.

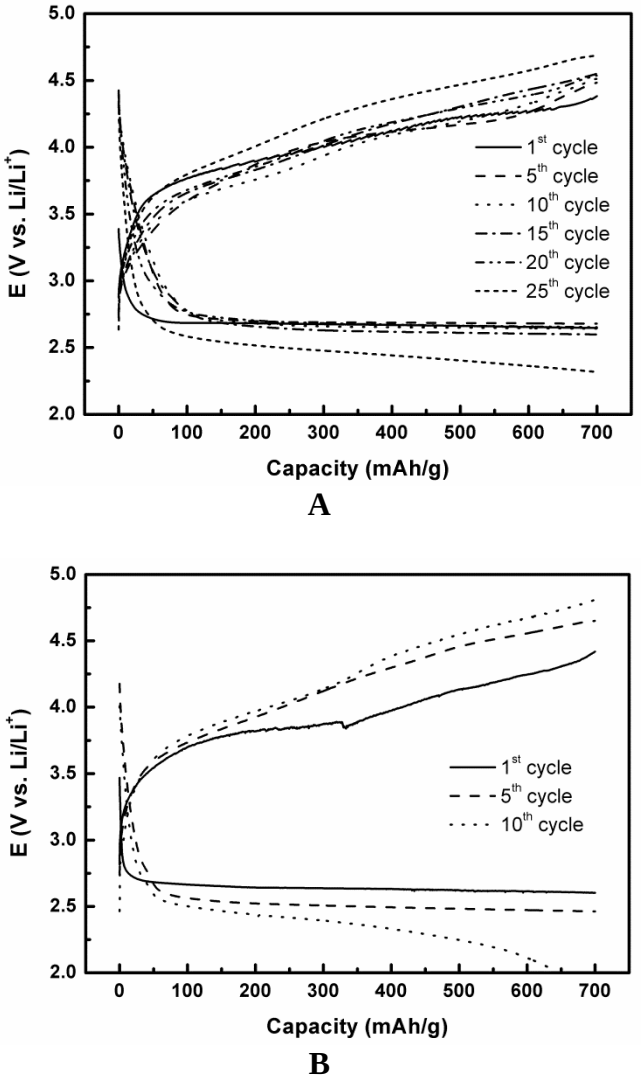

Figure 5. Charge-discharge profiles of (a) $Co(OH)_2$-$Fe(OH)_2$/CMK-3 and (b) $Co(OH)_2$-$Fe(OH)_2$/C catalysts on GDL in 1M LiTFSI in TEGDME electrolyte. Capacity was calculated by weight of catalyst in the electrode. Cycling was carried out at a current density of 157 mg/cm^2 (0.2 mA/g) and a cut-off capacity of 700 mAh/g.

Fig. 5 shows the results of charge-discharge testing for $Co(OH)_2$-$Fe(OH)_2$/CMK-3 catalyst as a cell cathode for Li-air batteries in order to confirm its electrocatalytic activity. All cell was cycled at current density of 0.2mg/cm^2 (157 mA/g) and cut-off capacity of 700 mAh/g. The electrolyte used ether-based 1M LiTFSI in TEGDME. In recent studies, although ether-based electrolytes were decomposed to Li_2CO_3, HCO_2Li, polyethers/ester, CO_2 and H_2O similar to carbonate-based electrolyte [28], they were often used the Li-air battery system due to its very high cell stability [29]. Fig. 5a shows the charge-discharge curve of $Co(OH)_2$-$Fe(OH)_2$/CMK-3 catalyst and the charge-discharge curve of catalyst which used carbon (Vulcan XC-72) as a supporting material instead of mesoporous carbon, $Co(OH)_2$-$Fe(OH)_2$/C is shown in Fig 5b. $Co(OH)_2$-$Fe(OH)_2$/CMK-3 catalyst has a plateau

region between 2.7 - 2.8 V in the first discharging and it slowly decreased until 20th cycle. The potential of the first charge process appeared 4.3 V at 700 mAh/g and increased during the process, finally it reached 4.6 V at 25th cycle. Compare to this results, $Co(OH)_2$-$Fe(OH)_2$/C catalyst as shown in Fig. 5b indicated a plateau region between 2.6 - 2.7 V in the first discharging. However, it quickly decreased, leading to the plateau region disappearing at 10th cycle. The potential of the first charge process appeared 4.4 V and increased during the cycling. Eventually, the charge potential of 4.7 V was observed at 10th cycle. As a result of the above cycling tests, both cycleability and overpotential of charge-discharge process were varied by the different supporting materials even though same catalysts with cobalt and iron hydroxide were adapted to Li-air battery. This is because the properties of mesopores and mesoporous material can have not only the high active sites by high volume and large surface area, but also the advantage for electron delivery to active center since continuous framework structures [30]. Moreover, the presence of mesopores was not only easy to diffuse the oxygen as a cathode, but also effective for the decomposition of discharge product because forming gases when lithium carbonates were broken down into H_2O and CO_2 during the discharging process were favorable to diffusion [25]. Therefore, the $Co(OH)_2$-$Fe(OH)_2$ catalyst on mesoporous carbon can decrease the overpotential during charging and discharging process, and improved cycleability compared to the carbon-supported catalysts.

In order to figure out the discharge products, the catalyst loaded on GDL was investigated by XRD analysis after 1st discharge and 1st charge process, respectively, as shown in Fig 6. Although discharge product of Li_2O_2 was not identified most detected peak in all specimens since catalyst peaks coincided with GDL peaks.

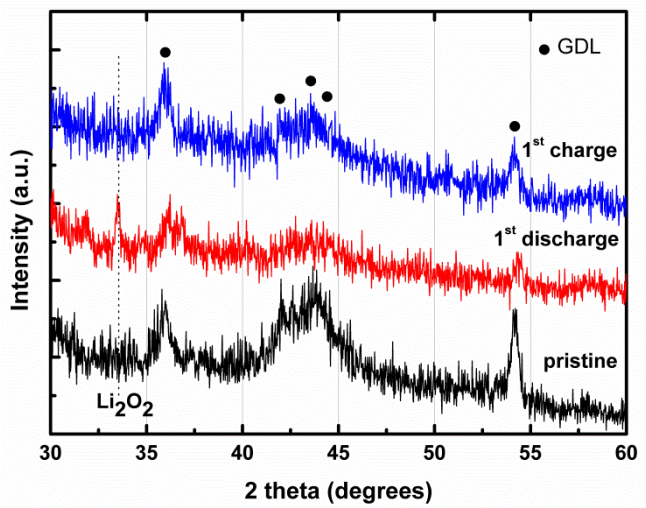

Figure 6. Comparison of X-ray diffraction (XRD) of $Co(OH)_2$-$Fe(OH)_2$/CMK-3 catalyst between the pristine, the 1st discharge and the 1st charge process.

However, the peak at ca. 33 2θ was able to be observed a clear separation. The peak was not detected at pristine status. It was showed after discharging process and finally disappeared after charging process. Therefore, it is certain that $Co(OH)_2$-$Fe(OH)_2$/CMK-3 catalyst can reversibly occur

formation and decomposition of discharge product, Li_2O_2 [31]. Furthermore, formation and decomposition of Li_2CO_3 was measured by FT-IR as shown in Fig. 7 [31].

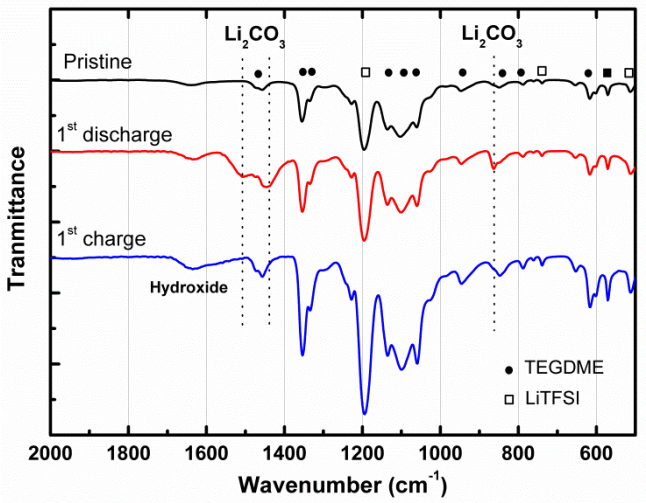

Figure 7. FT-IR spectra of $Co(OH)_2$-$Fe(OH)_2$/CMK-3 catalyst for the pristine, 1st discharge and 1st charge in 1M LiTFSI in TEGDME electrolyte.

The formation of Li_2CO_3 was found after the 1st discharging, which was also discharge product. The peaks, however, were also disappeared after charging [32]. Of course, the peaks of Li_2O_2 should be observed, but it was not appeared because the peaks of Li_2O_2 were overlapped with the peak of TEGDME having high transmittance.

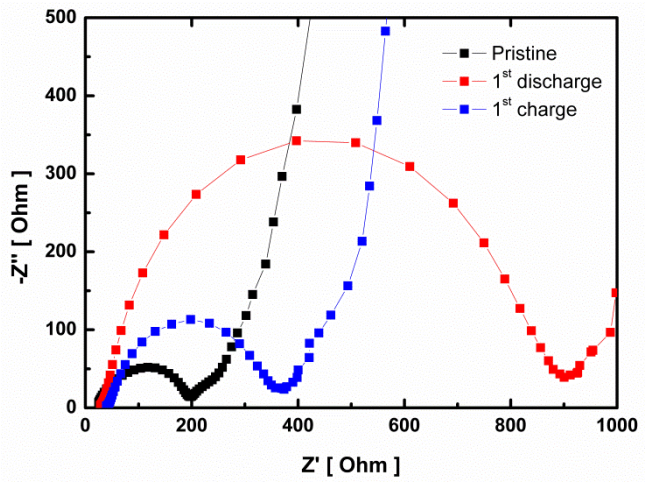

Figure 8. Electrochemical impedance spectroscopy (EIS) of $Co(OH)_2$-$Fe(OH)_2$/CMK-3 catalyst for the pristine, after the 1st discharge, and after the 1st charge.

In addition, EIS (electrochemical impedance spectroscopy) data as shown in Fig. 8 also can confirm that discharge products such as Li_2O_2, Li_2CO_3 were formed and decomposed during 1st charge-discharge process, resulting from the measurement of charge transfer resistance. The semi-circle after the 1st charge process was immensely decreased in comparison with the 1st discharge

process. Although the charge transfer resistance was higher than that of pristine, it can be confirmed that most of the discharge products were decomposed. Carbonate compounds, Li_2CO_3, formed during discharging mostly decomposed to CO_2 and H_2O. Afterwards, these gases were diffused to outside. Thus, CMK-3 supported catalysts can show the high cycleability compared to that of carbon-supported catalysts [33].

4. CONCLUSION

In this work, we investigated in detail the electrochemical and physical properties of the $Co(OH)_2$-$Fe(OH)_2$/CMK-3 catalyst prepared by modified polyol method as a cathode catalyst for Li-air batteries. The use of CMK-3 mesoporous carbon with cobalt and iron binary hydroxides catalyst significantly increases cycleability, capacity, and decreases overpotential during charging-discharging process due to the large catalytic active site. Electrochemical and physical analysis results confirm that mesopore of CMK-3 is advantageous: the efficient diffusion of oxygen during discharge process and the easy decomposition of discharge products, such as Li_2O_2 and Li_2CO_3, during charge process. Thus, the results can suggest that $Co(OH)_2$-$Fe(OH)_2$/CMK-3 having a high OER activity is a very effective catalyst to reduce the overpotential and to increase the cycleability for in non-aqueous Li-air batteries.

ACKNOWLEDGEMENT
This work was supported by the National Research Foundation of Korea Grant Funded by the Korean Government (MEST) (NRF-2012-M1A2A2671765).

References

1. A. S. Arico, P. Bruce, B. Scrosati, J. M. Tarascon, W. Schalkwijk, *Nat. Mater.* 4 (2005) 366.
2. M. Armand, J. M. Tarascon, *Nature*, 451 (2008) 652.
3. J. Wu, H. W. Park, A. Yu, D. Higgins, Z. Chen, *J. Phys. Chem. C.* 116 (2012) 9427.
4. J. M. Tarascon, M. Armand, Nature, 414 (2001) 359.
5. A. Taniguchi, N. Fujioka, M. Ikoma, A. Ohta, *J. Power Sources*, 100 (2001) 117.
6. Y. C. Lu, H. A. Gasteiger, E. Crumlin, J. R. Mcgure, Y. S. Horn, *J. Electrochem. Soc*. 157 (2010) A1016.
7. C. Terashima, Y. Iwai, S. P. Cho, T. Ueno, N. Zettsu, N. Saito, and O. Takai, *Int. J. Electrochem. Sci*., 8 (2013) 5407
8. Y. Ch. Lu, Z. Xu, H. A. Gasteiger, S. Chen, K. H. Schifferli, Y. S. Horn, *J. Am. Chem. Soc.* 132 (2010) 12170.
9. Y. Xing, Y. Cai, M.B. Vukmirovic, W.-P. Zhou, H. Karan, J.X. Wang, R.R. Adzic, J. *Phys. Chem. Lett.*, 1 (2010) 3238.
10. K. Huang, Y. Li, Y. Xing, *Electrochimica Acta*, 103 (2013) 44
11. A. Debart, A. J. Paterson, J. Bao and P. G. Bruce, *Angew. Chem., Int. Ed.* 47 (2008) 4521.
12. V. M. B. Crisostomo, J. K. Ngala, S. Alia, A. Dobley, C. Morein, C. H. Chen, X. Shen and S. L. Suib, *Chem. Mater.* 19 (2007) 1832.
13. T. Nissinen, Y. Kiros, M. Gasik, and M. Lampinen, *Mater. Res. Bull.* 39 (2004) 1195.
14. G. Wu, N. Li, D. R. Zhou, K. Mitsuo, and B. Q. Xu, *J. Solid State Chem.*, 177 (2004) 3682.

15. Y. G. Wang and H. S. Zhou, *J. Power Sources*, 195 (2010) 358.
16. B. A. Lu, D. X. Cao, P. Wang, G. L. Wang, and Y. Y. Gao, *Int. J. Hydrog. Energy*, 36 (2011) 72.
17. J. Xiao, J. Wnag, X. Li, J. Liu, D. Geng, J. Yang, Y. Li, L. Sun, *J. Electrochem. Soc.* 157 (2010) A487.
18. D. Y. Zhao, J. L. Feng, Q. S. Huo, N. Melosh, G. H. Fredrickson, B. F. Chmelka, G. D. Stucky, *Science*, 270 (1998) 548.
19. V. Shilapuram, N. Ozalp, M. Oschatz, L. Borchardt, S. Kaskel, Carbon, 67 (2014) 377.
20. D. Barrera, M. Davila, V. Cornette, J. C. A. Oliveira, R. H. Lopez, K. Sapag, Microporous and Mesoporous Materials, 180 (2013) 71.
21. M. Kruk, M. Jaroniec, S. H. Joo, R. Ryoo, *J. Phys. Chem. B* 107 (2003) 2205.
22. S. Jun, S. Joo, R. Ryoo, M. Kruk, M. Jaroniec, Z. Liu, T. Ohsuna, O. Terasaki, *J. Am. Chem. Soc*., 122 (2000) 10712.
23. Z. Zhou, S. Wang, W. Zhou, G. Wang, L. Jiang, W. Li, S. Song, J. Liu, G. Sun, Q Xin, *Chem. Commun.*, 4 (2003) 394.
24. B. Sun, H. Liu, P. Munroe, H. Ahn, G. Wang, *Nano Res.* 5 (2012) 460.
25. R. S. Assary, K. C. Lau, K. Amine, Y. K. Sun, L. A. Curtiss, *J. Phys. Chem. C*, 117 (2013) 8041.
26. G.A. El-Shobaky, F.H.A Abdalla, A.M. Ghozza, *Thermochimica Acta*, 292 (1997), 123.
27. T. Zhu, J. S. Chen, X. W. Lou, J. Phys. Chem. C, 115 (2011) 9814.
28. S. A. Freunberger, Y. Chen, N. E. Drewett, L. J. Hardwick, F. Barde, P. G. Bruce, *Angew. Chem. Int. Ed.*, 50 (2011) 8609.
29. R. Younesi, M. Hahlin, F. Bjorefors, P. Johansson, K. Edstrom, *Chem. Mater*., 25 (2013) 77.
30. S. H. Oh, R. Black, E. Pomerantseva, J. H. Lee, L. F. Nazar, *Nature chemistry*, 4 (2012) 1004.
31. G. Wu, N. H. Mack, W. Gao, R. Zhong, J. Han, J. K. Baldwin, P. Zelenay, *ACS Nano* 11 (2012) 9764.
32. R. S. Assary, J. Lu, P. Du, X. Luo, X. Zhang, Y. Ren, L. A. Curtiss, K. Amine, *Chem. Sus. Chem*. 6 (2013) 51
33. M. O. Thotiyl, S. A. Freunberger, Z. Peng, P. G. Bruce, *J. Am. Chem. Soc.* 135 (2103) 494.